LU Implicit Multigrid Algorithm for the Three-Dimensional Euler Equations

Jeffrey W. Yokota*
NASA Lewis Research Center, Cleveland, Ohio
and
D. A. Caughey†
Cornell University, Ithaca, New York

An LU implicit multigrid scheme is developed for the calculation of three-dimensional transonic flow through rotating cascades. This numerical method solves the unsteady Euler equations in finite-volume form with added adaptive artificial dissipation. The implicit scheme allows one to take a much larger time step than is normally permitted in most explicit schemes, while the multigrid method is incorporated to accelerate the convergence rate for steady-state calculations. Using this method, computational storage requirements are comparable to those of explicit schemes, while operation counts are considerably less than those found in the more widely used alternating direction implicit schemes.

Introduction

WITH the advent of supercomputers, fully three-dimensional aerodynamic calculations are quickly entering the realm of practicality. Many flow problems can be sufficiently investigated using two- and quasi-three-dimensional methods, but clearly many more existing problems require the use of fully three-dimensional analyses. This is particularly true of flows in turbomachinery where an incorrect axisymmetric solution can be produced from a quasi-three-dimensional analysis.[1]

In the present work, an lower-upper (LU) implicit multigrid scheme has been developed for the three-dimensional unsteady Euler equations of gas dynamics and applied to problems of transonic flow through rotating cascades. The LU factorization, proposed by Jameson and Turkel[2] and applied to two-dimensional problems by Buratynski and Caughey,[3] produces a scheme requiring two implicit inversions, each of which is solved by an effectively explicit sweep through the three-dimensional domain. This scheme has storage requirements comparable to those of explicit methods and the advantage of requiring only two point-implicit inversions as opposed to the three line-implicit inversions necessary in alternating direction implicit (ADI) schemes.[4,5] Time steps larger than those allowed in most explicit schemes can be used because of the LU scheme's large stability bounds, whereas a multigrid strategy is implemented to overcome the slower steady-state convergence rates often associated with using large time steps in approximately factored implicit schemes.[6] Results show the feasibility of using the LU scheme to solve the three-dimensional unsteady Euler equations and its ability to accelerate implicit Euler calculations to steady state when coupled with the multigrid method.

Analysis

To take advantage of the theoretical analysis available for systems of hyperbolic partial-differential equations, a time marching scheme is developed for the unsteady Euler equations. Systems of hyperbolic partial-differential equations propagate information through their prescribed domains by means of characteristic wave speeds of different magnitudes and signs. This would suggest the attractiveness of an implicit numerical scheme since, unlike most explicit methods, the stability of implicit schemes is not limited by these characteristic wave speeds. The equations are written in divergence form and then transformed to a generalized coordinate system that is fixed relative to the rotating cascade. The resulting system of equations, incorporating the equation of state for a perfect gas, can be written in nondimensional form as follows:

$$\frac{\partial W}{\partial t}+\frac{\partial F}{\partial \xi}+\frac{\partial G}{\partial \eta}+\frac{\partial H}{\partial \zeta}=S \tag{1}$$

For a constant cascade rotation of $\omega=\omega k$

$$W=\begin{bmatrix} \rho D \\ \rho Du \\ \rho Dv \\ \rho Dw \\ DR \end{bmatrix}, \quad F=\begin{bmatrix} \rho DU \\ \rho DUu+P(y_\eta z_\zeta - y_\zeta z_\eta) \\ \rho DUv+P(x_\zeta z_\eta - x_\eta z_\zeta) \\ \rho DUw+P(x_\eta y_\zeta - x_\zeta y_\eta) \\ DU(R+P) \end{bmatrix}$$

$$G=\begin{bmatrix} \rho DV \\ \rho DVu+P(y_\zeta z_\xi - y_\xi z_\zeta) \\ \rho DVv+P(x_\xi z_\zeta - x_\zeta z_\xi) \\ \rho DVw+P(x_\zeta y_\xi - x_\xi y_\zeta) \\ DV(R+P) \end{bmatrix}$$

$$H=\begin{bmatrix} \rho DW \\ \rho DWu+P(y_\xi z_\eta - y_\eta z_\xi) \\ \rho DWv+P(x_\eta z_\xi - x_\xi z_\eta) \\ \rho DWw+P(x_\xi y_\eta - x_\eta y_\xi) \\ DW(R+P) \end{bmatrix}, \quad S=\begin{bmatrix} 0 \\ \rho D\omega(2v+\omega x) \\ \rho D\omega(-2u+\omega y) \\ 0 \\ 0 \end{bmatrix}$$

Received May 9, 1987; revision received Sept. 21, 1987.

*Research Engineer, Sverdrup Technology, Inc. Member AIAA.
†Professor, Sibley School of Mechanical and Aerospace Engineering. Associate Fellow AIAA.

where the variables t, ρ, u, v, w, and P represent time, density Cartesian relative flow velocity components, and pressure. The relative Cartesian coordinates are represented as x, y, z whereas the transform relative general coordinates are defined as ξ, η, ζ.

In terms of the transformation matrices

$$J = \begin{bmatrix} x_\xi & x_\eta & x_\zeta \\ y_\xi & y_\eta & y_\zeta \\ z_\xi & z_\eta & z_\zeta \end{bmatrix}$$

$$J^{-1} = \begin{bmatrix} \xi_x & \xi_y & \xi_z \\ \eta_x & \eta_y & \eta_z \\ \zeta_x & \zeta_y & \zeta_z \end{bmatrix}$$

$$= \frac{1}{D} \begin{bmatrix} y_\eta z_\zeta - y_\zeta z_\eta & x_\zeta z_\eta - x_\eta z_\zeta & x_\eta y_\zeta - x_\zeta y_\eta \\ y_\zeta z_\xi - y_\xi z_\zeta & x_\xi z_\zeta - x_\zeta z_\xi & x_\zeta y_\xi - x_\xi y_\zeta \\ y_\xi z_\eta - y_\eta z_\xi & y_\eta z_\xi - x_\xi z_\eta & x_\xi y_\eta - x_\eta y_\xi \end{bmatrix}$$

where D is determinant of matrix J. The contravariant velocities can be defined as

$$\begin{bmatrix} U \\ V \\ W \end{bmatrix} = J^{-1} \begin{bmatrix} u \\ v \\ w \end{bmatrix}$$

where

$$R = \rho\left[\epsilon + \frac{V \cdot V}{2} - \frac{(\omega \times r)\cdot(\omega \times r)}{2}\right]$$

$R + P$ = Rothalpy, r = relative position vector, and ϵ = internal energy.

$$P = (\gamma - 1)\left\{R - \rho\left[\frac{V \cdot V}{2} - \frac{(\omega \times r)\cdot(\omega \times r)}{2}\right]\right\}$$

The Euler equations are solved in these transformed relative coordinates to take advantage of the fact that the flow is steady in this reference frame. Since the physical boundaries can be made to coincide with transformed coordinate surfaces, a one-dimensional analysis normal to the boundary can be incorporated. Following the theory developed by Kreiss[7,8] for systems of one-dimensional hyperbolic partial-differential equations, the number of conditions specified at a given boundary is equal to the number of characteristic waves entering into the domain. To close the computational boundary problem, the unspecified conditions are taken to be the compatibility relations corresponding to the outgoing characteristic waves. The one-dimensional compatibility relations are

$$\frac{\partial P}{\partial \psi} - c^2 \frac{\partial \rho}{\partial \psi} = 0 \tag{2a}$$

$$\frac{\partial u}{\partial \psi} - \frac{\zeta_x}{\zeta_z}\frac{\partial w}{\partial \psi} = \omega(2v + \omega x) \tag{2b}$$

$$\frac{\partial v}{\partial \psi} - \frac{\zeta_y}{\zeta_z}\frac{\partial w}{\partial \psi} = \omega(-2u + \omega y) \tag{2c}$$

$$\frac{\partial P}{\partial \phi} - \frac{\rho c^2 \zeta_x}{\tilde{C}}\frac{\partial u}{\partial \phi} - \frac{\rho c^2 \zeta_y}{\tilde{C}}\frac{\partial v}{\partial \phi} - \frac{\rho c^2 \zeta_z}{\tilde{C}}\frac{\partial w}{\partial \phi}$$

$$= -\frac{\rho c^2 \omega}{\tilde{C}}[\zeta_x(2v + \omega x) + \zeta_y(-2u + \omega y)] \tag{2d}$$

$$\frac{\partial P}{\partial \sigma} + \frac{\rho c^2 \zeta_x}{\tilde{C}}\frac{\partial u}{\partial \sigma} + \frac{\rho c^2 \zeta_y}{\tilde{C}}\frac{\partial v}{\partial \sigma} + \frac{\rho c^2 \zeta_z}{\tilde{C}}\frac{\partial w}{\partial \sigma}$$

$$= \frac{\rho c^2 \omega}{\tilde{C}}[\zeta_x(2v + \omega x) + \zeta_y(-2u + \omega y)] \tag{2e}$$

where

$$\frac{\partial}{\partial \psi} = \frac{\partial}{\partial t} + W\frac{\partial}{\partial \zeta}$$

$$\frac{\partial}{\partial \phi} = \frac{\partial}{\partial t} + (W - \tilde{C})\frac{\partial}{\partial \zeta}$$

$$\frac{\partial}{\partial \sigma} = \frac{\partial}{\partial t} + (W + \tilde{C})\frac{\partial}{\partial \zeta}$$

$$\tilde{C} = \frac{c}{D}[(y_\xi z_\eta - y_\eta z_\xi)^2 + (x_\eta z_\xi - x_\xi z_\eta)^2 + (x_\xi y_\eta - x_\eta y_\xi)^2]^{1/2}$$

Thus, the computational boundary problem requires a simultaneous solution of the incoming specified conditions and the outgoing compatibility relations. For a subsonic cascade inflow, the specified conditions are total pressure, total temperature, and the relative inflow angles to the ξ-ζ and η-ζ planes. For a subsonic cascade outflow, the specified boundary condition is chosen to be a nonreflective condition, similar to that of Rudy and Stirkwerda,[9] that minimizes unwanted reflected waves from the subsonic relative outflow boundary. This nonreflective condition is based on a linear combination of the unsteady terms in the incoming compatibility relation and specified static pressure calculated from radial equilibrium.

$$\frac{\partial P}{\partial t} - \frac{\rho \tilde{C}}{\zeta_z}\frac{\partial w}{\partial t} + \beta(P - P_{ex}) = 0 \tag{3}$$

where the scalar constant $\beta \geq 0$, and P_{ex} is the static pressure calculated from radial equilibrium.

Geometric considerations dictate that the flow fore and aft of the blades be periodic while the solid boundaries require no-flux conditions.

Discretization

The transformed unsteady Euler equations are approximated by finite-difference equations using a finite-volume formulation. Flux-embedded geometric quantities, equivalent to surface projections, are produced from the generalized transformation and evaluated on the faces of each grid cell. This treatment of the geometric terms prevents the production of geometrically induced truncation errors and allows for the admission of possible uniform flow solutions. This requires that both the flow variable and the flux-embedded geometric quantities be defined on the faces of the grid cells during the flux calculations, although it is cell-averaged values that are calculated during time and spatial marching.

The unsteady equations can be discretized into an implicit scheme

$$\frac{\Delta W^n}{\Delta t} + \mu(\delta_\xi F_{ijk} + \delta_\eta G_{ijk} + \delta_\zeta H_{ijk} - S_{ijk})^{n+1}$$

$$+ (1 - \mu)(\delta_\xi F_{ijk} + \delta_\eta G_{ijk} + \delta_\zeta H_{ijk} - S_{ijk})^n = 0 \tag{4}$$

where $\Delta W^n = W^{n+1} - W^n$, Δt is the time step size, and $0 \le \mu \le 1$ is a parameter governing the degree of implicitness. A Taylor series linearization about time level n gives

$$F^{n+1}_{ijk} = F^n_{ijk} + A^n_{ijk} \Delta W^n_{ijk}$$

This (together with similar linearizations for G, H, and S) can be used to write the implicit system in the linearized delta form

$$[I + \mu \Delta t(\delta_\xi A + \delta_\eta B + \delta_\zeta C - E)]\Delta W^n_{ijk}$$
$$= -\Delta t(\bar{\delta}_\xi F_{ijk} + \bar{\delta}_\eta G_{ijk} + \bar{\delta}_\zeta H_{ijk} - S_{ijk})^n \quad (5)$$

where the Jacobian matrix $E = \partial s/\partial w$, I is the identity matrix, and δ and $\bar{\delta}$ are cell-centered and face-centered central differences of the form

$$\delta_\xi \phi = (\phi_{i+1} - \phi_{i-1})/2, \quad \bar{\delta}_\xi \phi = \phi_{i+1/2} - \phi_{i-1/2}$$

Artificial Dissipation

The implicit system of equations is written in delta form to produce a scheme whose steady-state solutions are independent of the time step sizes used in the time marching. The finite-volume formulation reduces to a centered-difference approximation on a uniform grid and thus requires the addition of explicit artificial dissipation terms to suppress possible odd and even point oscillations and shock overshoots. The explicit artificial directional dissipation added is a blended nonlinear second- and fourth-difference term similar to that of Jemeson,[10] but with a modified one-dimensional scaling factor that adds properly scaled terms in each of the three coordinate directions. This attempts to add only as much dissipation as is needed in each direction. The dissipation term is of the form

$$T_{ijk} - \bar{\delta}_\xi K^{(2)}_i D \delta_\xi \frac{1}{D} W_{ijk} + \bar{\delta}_\xi K^{(4)}_i D \delta_{\xi\xi\xi} \frac{1}{D} W_{ijk} \quad (6)$$

where the ξ-direction terms are defined as follows. The difference operators $\bar{\delta}_\xi$ are face-centered central first differences, while $\bar{\delta}_{\xi\xi\xi}$ are face-centered central third differences. The nonlinear scaling factor found in the second-difference term is

$$K^{(2)}_{i+1/2} = \frac{X^{(2)}}{\Delta t'_{i+1/2}} \nu_{i+1/2}$$

and the blended scaling factor found in the fourth-difference term is

$$K^{(4)}_{i+1/2} = \max\left(0, \frac{X^{(4)}}{\Delta t'_{i+1/2}} - K^{(2)}_{i+1/2}\right)$$

where $X^{(2)}$ and $X^{(4)}$ are scalar constants. The shock-sensing term is defined as

$$\nu_{i+1/2} = \max(\nu_{i+2}, \nu_{i+1}, \nu_i, \nu_{i-1})$$

where

$$\nu_i = \left\| \frac{P_{i+1} - 2P_i + P_{i-1}}{P_{i+1} + 2P_i + P_{i-1}} \right\|$$

The critical time-scaling term is defined as

$$\Delta t'_{i+1/2} = \frac{\Delta \xi}{|A_{i+1/2}|}$$

where $\Delta \xi$ is the grid spacing in the ξ direction and the directional wave-speed term

$$|A_{i+1/2}| = \max(|\Lambda_A|_{i+1/2})$$

is defined as the absolute value of the maximum eigenvalue of the Jacobian matrix A and is evaluated directly on the cell faces.

Defining a second-difference artificial directional dissipation matrix operator,

$$Q = -\left[\bar{\delta}_\xi K^{(2)}_i D \delta_\xi \frac{1}{D} + \bar{\delta}_\eta K^{(2)}_j D \delta_\eta \frac{1}{D} + \bar{\delta}_\zeta K^{(2)}_k D \delta_\zeta \frac{1}{D}\right] I$$

the second-difference contributions to the explicit artificial dissipation are treated implicitly to produce the system

$$[I + \mu \Delta t(\delta_\xi A + \delta_\eta B + \delta_\zeta C - E + Q)]\Delta W^n_{ijk}$$
$$= -\Delta t(\bar{\delta}_\xi F_{ijk} + \bar{\delta}_\eta G_{ijk} + \bar{\delta}_\zeta H_{ijk} - S_{ijk} + T_{ijk})^n \quad (7)$$

LU Factorization

The linearized implicit operator produces a large, block-banded, matrix system that is impractical to solve. The most common way of dealing with this difficulty is to perform an approximate factorization on the block-banded implicit operator to reduce the large storage and operation counts that would otherwise be required for its solution. A central-differenced ADI factorization would produce a scheme with three block tridiagonal operators, whereas the one-sided differenced LU factorization produces two block triangular factors, one upper and one lower. The two block triangular factors produced in the LU scheme require significantly less storage than the ADI's three block tridiagonal factors and are less expensive to solve. An ADI scheme would require three line-implicit sweeps through the domain whereas the LU scheme requires only two effectively explicit sweeps through the flowfield. In addition, the LU scheme has the benefit of being stable in all dimensions[2] whereas ADI, at least in theory, is unstable in delta form for three-dimensional scalar hyperbolic equations.

The LU implicit scheme can be written as

$$[I + \mu \Delta t(\delta^-_\xi A_1 + \delta^-_\eta B_1 + \delta^-_\zeta C_1 - E_1 + Q_1)]$$
$$\cdot [I + \mu \Delta t(\delta^+_\xi A_2 + \delta^+_\eta B_2 + \delta^+_\zeta C_2 - E_2 + Q_2)]\Delta W^n_{ijk}$$
$$= -\Delta t(\bar{\delta}_\xi F_{ijk} + \bar{\delta}_\eta G_{ijk} \bar{\delta}_\zeta H_{ijk} - S_{ijk})^n \quad (8)$$

where δ^+ and δ^- are cell-centered forward and backward first differences, respectively, and the implicit splittings of the Jacobian matrices are defined such that

$$A_1 + A_2 = A, \qquad B_1 + B_2 = B$$
$$C_1 = C_2 = C, \qquad E_1 + E_2 = E$$
$$Q_1 + Q_2 = Q$$

A number of different LU factorizations, each characterized by different implicit operator splittings, have been proposed. Steger and Warming's[11] flux-vector splitting schemes are based on a directional eigenvalue splitting whereas Pan and Lomax[12] proposed a preconditioned diagonal operator in each of the lower and upper factors. The splitting used in this work is based on the Jameson and Turkel splitting[2] where the Jacobian matrices A, B, and C are split and reconstructed to produce diagonally dominant factors for each matrix inversion in every cell. This is ensured by making the eigenvalue of the forward-differenced reconstructed Jacobian matrices non-

positive and the eigenvalues of the backward-differenced reconstructed Jacobian matrices nonnegative. The source Jacobian matrix E is split evenly between the upper and lower factors, whereas the dissipation operator Q is split in a manner consistent with the differencing of the Jacobian matrices A, B, and C. Thus,

$$A_1 = \frac{(A + |A|I)}{2}, \qquad A_2 = \frac{(A - |A|I)}{2}$$

$$B_1 = \frac{(B + |B|I)}{2}, \qquad B_2 = \frac{(B - |B|I)}{2}$$

$$C_1 = \frac{(C + |C|I)}{2}, \qquad C_2 = \frac{(C - |C|I)}{2}$$

$$E_1 = \frac{E}{2}, \qquad E_2 = \frac{E}{2}$$

$$Q_1 = + \left[K^{(2)}_{l-\frac{1}{2}} D \delta^-_\xi \frac{1}{D} \right] I$$

$$Q_2 = - \left[K^{(2)}_{l+\frac{1}{2}} D \delta^+_\xi \frac{1}{D} \right] I$$

where

$$|A| = \max(|\Lambda_A|) \qquad \text{etc. ...}$$

The effect of the Jacobian matrix splittings can be thought of as an additional constant-coefficient second-difference artificial dissipation-like term in the implicit operator. This dissipation-like operator would take the form

$$\tilde{Q} = - \left[\delta_{\xi\xi} \frac{|A|}{2} + \delta_{\eta\eta} \frac{|B|}{2} + \delta_{\zeta\zeta} \frac{|C|}{2} \right] I$$

The system of equations is solved in two steps:
Step 1 (lower sweep):

$$[I + \mu\Delta t(\delta^-_\xi A_1 + \delta^-_\eta B_1 + \delta^-_\zeta C_1 - E_1 + Q_1)]\Delta Y^n_{ijk}$$
$$= -\Delta t(\bar{\delta}_\xi F_{ijk} + \bar{\delta}_\eta G_{ijk} + \bar{\delta}_\zeta H_{ijk} - S_{ijk} + T_{ijk})^n \qquad (9)$$

The right-hand side of this system of equations is commonly referred to as the "residual" and is evaluated using the finite-volume formulation of the finite-difference equations. The system is solved by an effectively explicit sweep through the domain in the positive ξ, η, and ζ directions to produce the intermediate variable ΔY^n_{ijk} at each grid cell.

Step 2 (upper sweep):

$$[I + \mu\Delta t(\delta^+_\xi A_2 + \delta^+_\eta B_2 + \delta^+_\zeta C_2 - E_2 + Q_2)]\ \Delta W^n_{ijk} = \Delta Y^n_{ijk} \qquad (10)$$

Here the system is solved similarly by an effectively explicit sweep through the domain, but in opposite directions to the sweep taken in step 1. The flowfield corrections are produced at every grid cell and then used to update the flowfield.

Boundary Treatment

The residual calculation requires boundary values on the flowfield W, whereas the first and second steps of the LU procedure require implicit boundary values on the intermediate variables ΔY and the flowfield corrections ΔW, respectively.

As stated previously, the inflow/outflow boundary values are produced from a simultaneous solution of the incoming specified conditions and the outgoing compatibility relations. The compatibility relations are approximated by one-sided linearized finite-difference equations whose spatial diections are determined by the signs of the corresponding eigenvalues. These difference equations, together with the appropriate specified boundary conditions, are used to produce the flow variables at the inflow/outflow boundaries.

During the residual calculation, the no-flux condition is enforced at solid boundaries by setting to zero the contravariant velocity component corresponding to the normal flux. This treatment requires that only pressures need to be specified along solid boundaries and are obtained by a zeroth-order extrapolation normal to the boundary.

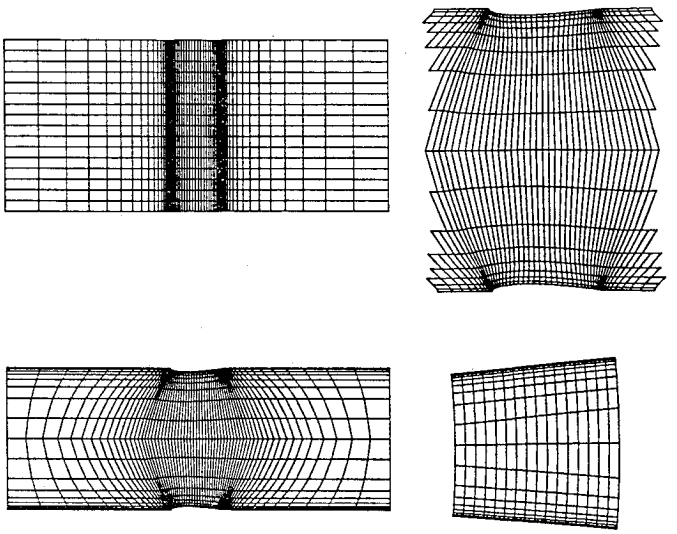

Fig. 1 Three-view drawing of three-dimensional grid with expanded view of blade-to-blade surface; NACA 0012 plane cascade 10, grid 16×16×64.

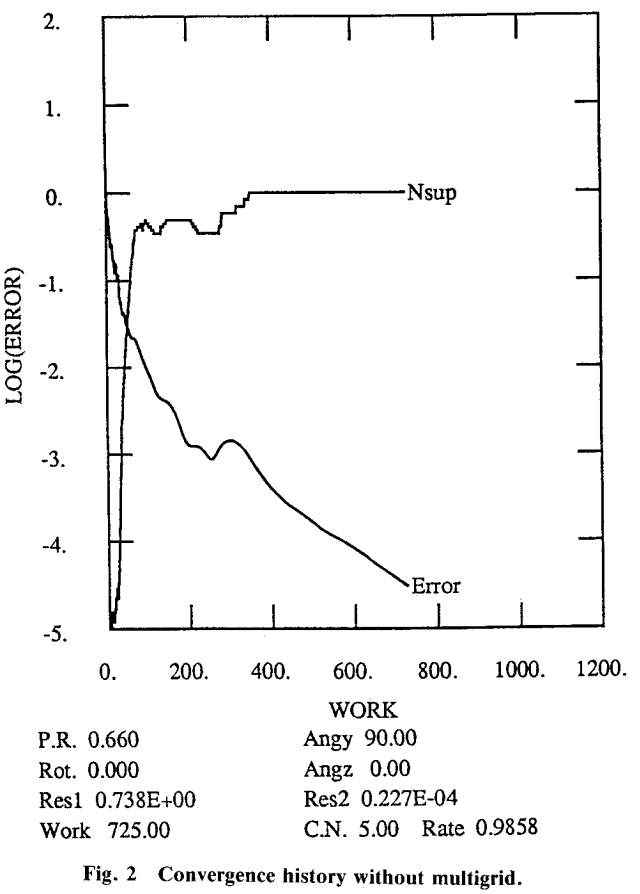

Fig. 2 Convergence history without multigrid.

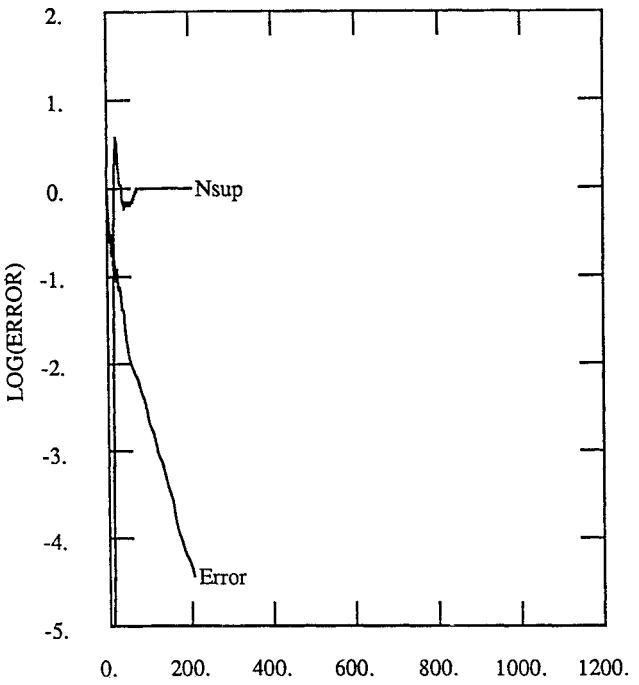

P.R. 0.660 Angy 90.00
Rot. 0.000 Angz 0.00
Res1 0.738E+00 Res2 0.272E-04
Work 206.00 C.N. 5.00 Rate 0.9516

Fig. 3 Convergence history with multigrid.

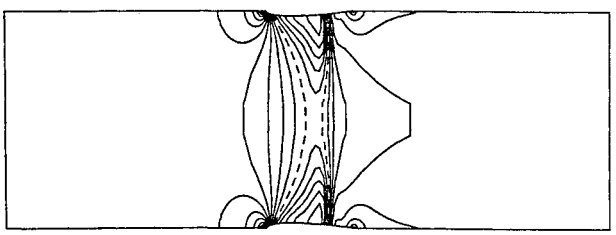

Mach Number Levels

0.400	0.600	0.800	1.000	1.200
0.450	0.650	0.850	1.050	1.250
0.500	0.700	0.900	1.100	
0.550	0.750	0.950	1.150	

Fig. 4 Relative Mach number on a blade-to-blade grid plane; NACA 0012 plane cascade 10, grid 16×16×64, 5.69% radius.

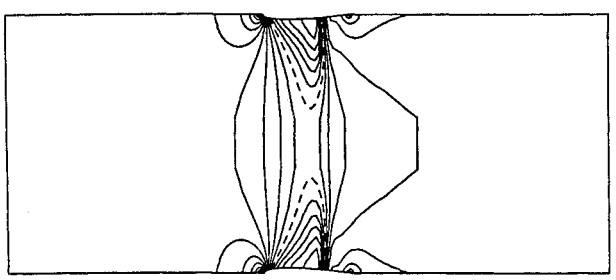

Mach Number Levels

0.400	0.600	0.800	1.000	1.200
0.450	0.650	0.850	1.050	1.250
0.500	0.700	0.900	1.100	
0.550	0.750	0.950	1.150	

Fig. 5 Relative Mach number on a blade-to-blade grid plane; NACA 0012 plane cascade 10, grid 16×16×64, 93.19% radius.

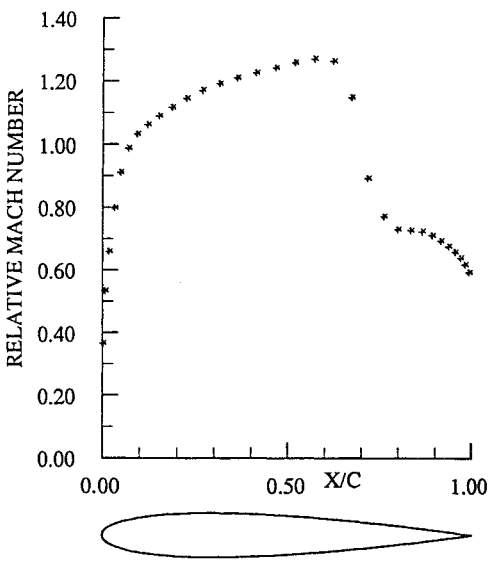

Fig. 6 Relative Mach number blade distribution; NACA 0012 plane cascade 10, 5.69% radius.

Flowfield corrections and intermediate variables are required at the inflow and outflow boundaries. Intermediate variables are needed at the inflow boundary prior to starting the lower sweep and are taken to be a linear combination of zeroth-order spatial and temporal extrapolations. Outflow flowfield corrections are required before starting the upper sweep and are obtained from the explicit calculation of the outflow flow variables. A periodic matrix solver (a four-step cyclic inversion that retains the explicit nature of the LU scheme)[3] is incorporated into the LU procedure between the periodic boundaries and thus does not require any specified boundary variables. An implicit treatment of the no-flux condition, which does not difference across solid boundaries, is incorporated to prevent the introduction of an artificial flux in the implicit field. This is equivalent to solving simultaneously for two points, one on either side of a solid boundary, with the specification that there be no flux across the solid boundary.

Initial conditions are needed to start the flow calculations; they can be either a uniform flow based on an initial guess or interpolated from a converged solution on a coarser grid.

Steady-State Calculations

The LU implicit scheme is coupled with local time stepping and the multigrid method to improve the convergence rates of steady-state calculations. Local time stepping is used to improve the propagation of information through the domain by optimizing the time step size throughout the flowfield. Thus, an optimum time step size is used at evey point in the domain to reduce the number of time steps required to reach a steady state. This produces a warped time integration but does not affect the steady-state solution.

Finally, a multigrid method following the work of South and Brandt[13] and Jameson and Yoon[14] is incorporated into the LU implicit scheme to accelerate the removal of low-frequency errors from the flow solution. The LU scheme acts to smooth out the components of the high-frequency error that are resolvable on any current grid level but unseen on subsequent coarser grids. The multigrid sequencing used is a three-level W-cycle that uses a double pass on the coarser grids as opposed to the standard single pass V-cycle.

To limit the amount of high-frequency error transferred to the fine grid from the coarser grids, the coarse grid residuals are kept smooth. This is accomplished by using only a constant-coefficient-explicit second-difference artificial dissipation term on the coarse grids rather than the nonlinear blended terms used on the fine grid. This constant term is not

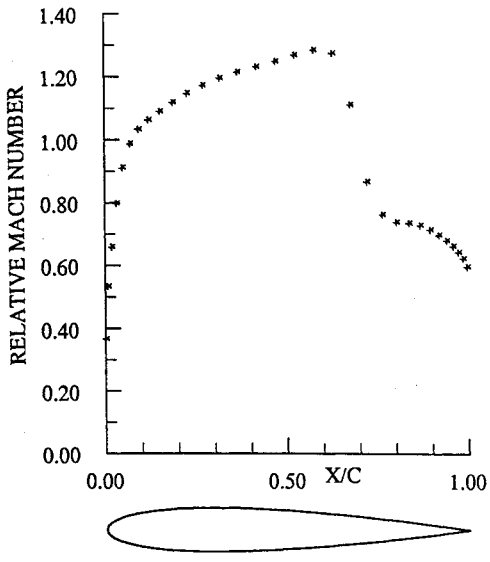

Fig. 7 Relative Mach number blade distribution; NACA 0012 plane cascade 10, 93.19% radius.

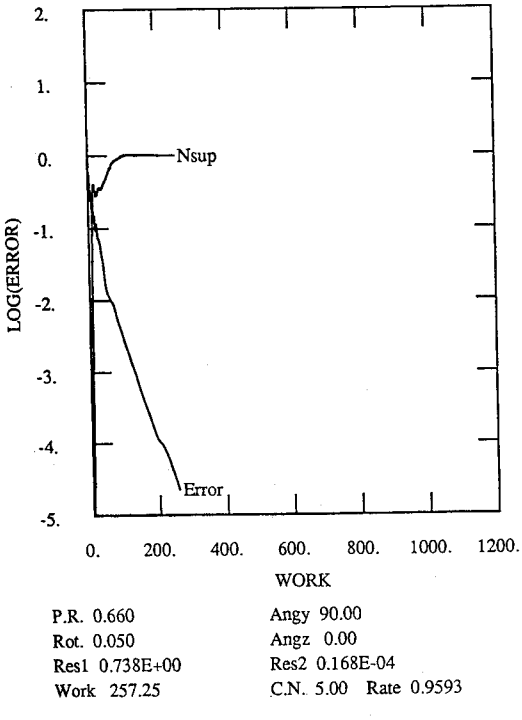

Fig. 8 Convergence history with multigrid.

treated implicitly due to the already existing implicit dissipation-like term produced by the Jacobian matrix splittings. Boundary conditions on the coarse grids are the same as on fine grids with the exception of the inflow/outflow conditions. To keep the mass flow identical on all grids, the inflow/outflow boundary conditions are updated only on the finest grid. The LU smoother is used only once during each flow calculation and no flow calculations are invoked after upward interpolations of the flowfield corrections.

Results

The first two test calculations were performed on a three-dimensional plane cascade developed from the NACA 0012 airfoil. The three-dimensional geometry is a 36-blade axial rotor with a 0.825 hub-to-tip radius ratio and a 14.3 tip radius-to-blade chord ratio. Transonic test cases were run for both rotating and stationary cascades at a Courant number of 5. Calculations were performed on a H-type grid containing $64 \times 16 \times 16$ mesh cells in the throughflow, blade-to-blade, and radial directions, respectively. The grid was generated using a modified version of the GRAPE code developed by Sorenson.[15] Figure 1 shows exploded blade-to-blade, hub-to-shroud, and axial passage planes with an expanded view of the blade-to-blade grid.

The first test case is a nonrotating cascade with a 0.66 exit static-to-inflow total pressure ratio and axial relative inflow. To illustrate the effects of multigrid, the convergence plots of two calculations, one with and one without the use of the multigrid method, are shown. Convergence histories are represented by plots of the logarithmic value of the error and a measure of the supersonic region in the flowfield. The error in the flowfield is represented by the root-mean-square (rms) rate of change of the continuity equation on the finest grid. The developing supersonic region is measured by the number of grid cells found to contain supersonic flow. These quantities are plotted vs a measure of the computational effort required to solve the discretized Euler equations. The computational effort is represented by a work unit that is normalized by a single LU calculation on the finest grid. Thus, 1 work unit is equivalent to 1 LU calculation on the finest grid, whereas calculations on two sequentially coarser grids have values of 1/8 and 1/64 of a work unit, respectively. Without taking into account the work required in the interpolation and transferring operations, a single multigrid step in a three-level W-cycle takes 41/32 of a work unit. The single grid calculation (see Fig. 2) shows a reduction in the rms averaged residual of about four-and-one-half orders of magnitude after 725 work units with the supersonic region fully developed after about 350 work units. The multigrid calculation (see Fig. 3) shows a reduction in the rms averaged residual at about four-and-one-half orders of magnitude within 200 work units and a fully developed supersonic region after 50 work units. Clearly, the convergence rates of steady-state implicit calculations can be significantly accelerated with the use of the multigrid method.

Figures 4 and 5 show plots of the relative Mach number field on blade-to-blade surfaces at stations of 5.69 and 93.19% hub-to-shroud radii with the corresponding blade surface distributions in Figs. 6 and 7. These results illustrate the LU implicit scheme's ability to resolve the transonic cascade flow and to produce symmetrical converged solutions in spite of the distinctly asymmetric nature of the iterative procedure.

A second test case has nondimensional rotation of 0.05 with a 0.66 exit static-to-inflow total pressure ratio and axial relative inflow. The rotation rate is nondimensionalized by the square root of the product of the specified total temperature and thermodynamic gas constant, divided by the blade chord. The convergence history is shown in Fig. 8 with the relative Mach number plots found in Figs. 9–13. The convergence rate of the rotating case is slightly slower than that of the nonrotating case, but again it can be seen that the multigrid procedure allows the flowfield to be established within 100 work units. Here the multigrid procedure was used to reduce the residual four-and-one-half orders of magnitude within 250 work units and produce a fully developed supersonic region within 150 work units. Figures 9 and 10 reveal a fully three-dimensional flow with a shock extending across the passage beside the hub and only slightly formed beside the shroud. The effects of the passage rotation are seen in the flowfield variations from hub to shroud (see Fig. 13). The coriolis effects are seen in the slight nonsymmetry produced in the blade-to-blade planes (see Figs. 11 and 12) despite the fully axial inflow in the relative frame.

The final test case is a calculation on a core compressor rotor designed at the NASA Lewis Research Center and designated as Rotor 33.[16] The three-dimensional geometry has a constant radius hub and a converging tip. The 52-blade compressor rotor has a tip radius of 254 mm, a tip chord of 44.5

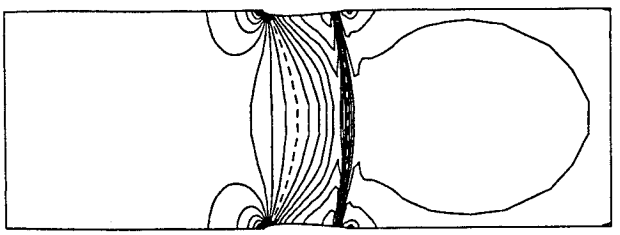

Mach Number Levels

0.400	0.600	0.800	1.000	1.200
0.450	0.650	0.850	1.050	1.250
0.500	0.700	0.900	1.100	1.300
0.550	0.750	0.950	1.150	1.350

Fig. 9 Relative Mach number on a blade-to-blade grid plane; NACA 0012 plane cascade 10, grid 16 × 16 × 64, 5.69% radius.

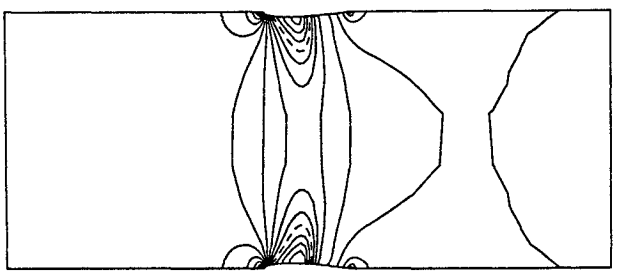

Mach Number Levels

0.400	0.600	0.800	1.000
0.450	0.650	0.850	1.050
0.500	0.700	0.900	1.100
0.550	0.750	0.950	1.150

Fig. 10 Relative Mach number on a blade-to-blade grid plane; NACA 0012 plane cascade 10, grid 16 × 16 × 64, 93.19% radius.

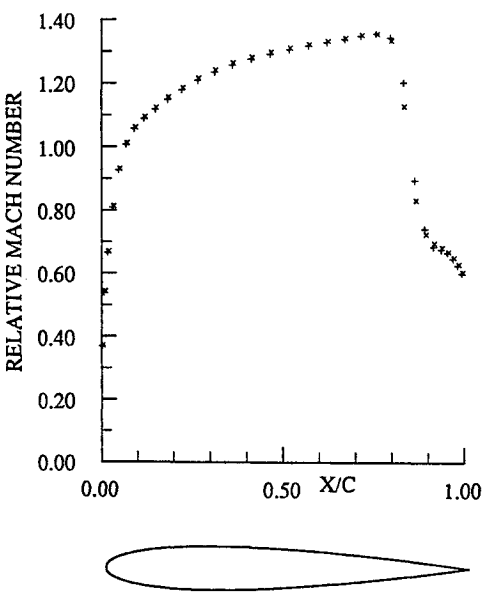

Fig. 11 Relative Mach number blade distribution; NACA 0012 plane cascade 10, 5.69% radius.

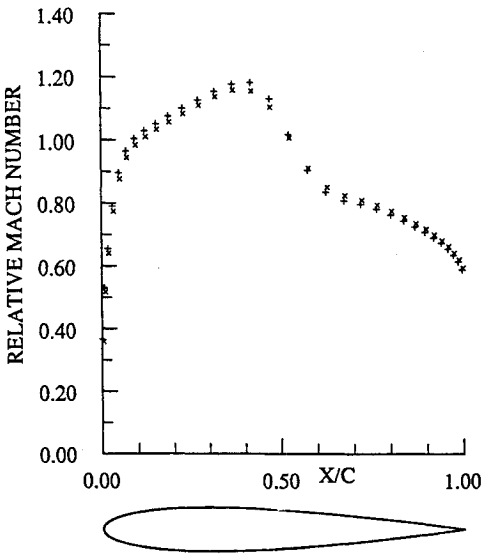

Fig. 12 Relative Mach number blade distribution; NACA 0012 plane cascade 10, 93.19% radius.

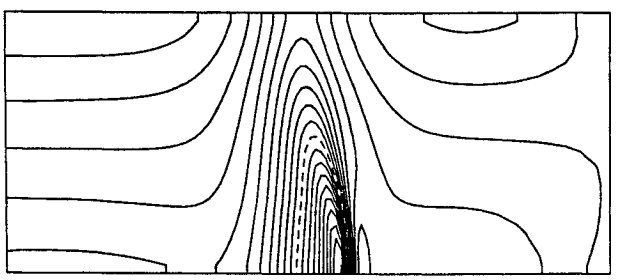

Mach Number Levels

0.725	0.825	0.925	1.025	1.125	1.225
0.750	0.850	0.950	1.050	1.150	
0.775	0.875	0.975	1.075	1.175	
0.800	0.900	1.000	1.100	1.200	

Fig. 13 Relative Mach number on a hub-to-shroud grid plane; NACA 0012 plane cascade 10, grid 16 × 16 × 24, 50% passage width.

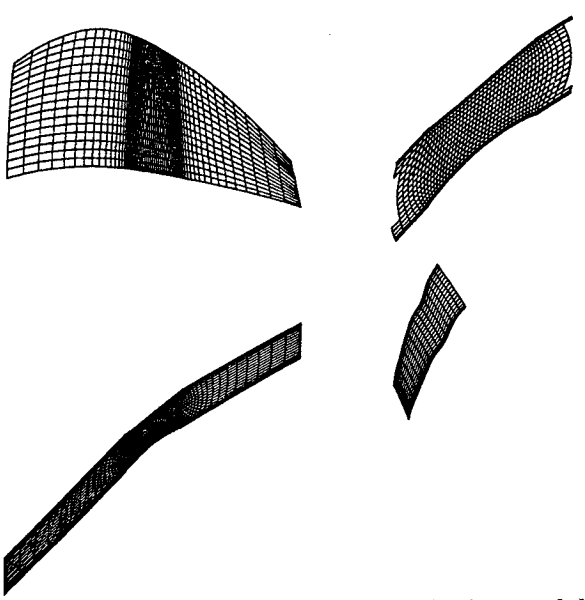

Fig. 14 Three-view drawing of three-dimensional grid with expanded view of blade-to-blade surface; rotor 33 compressor, grid 16 × 16 × 64.

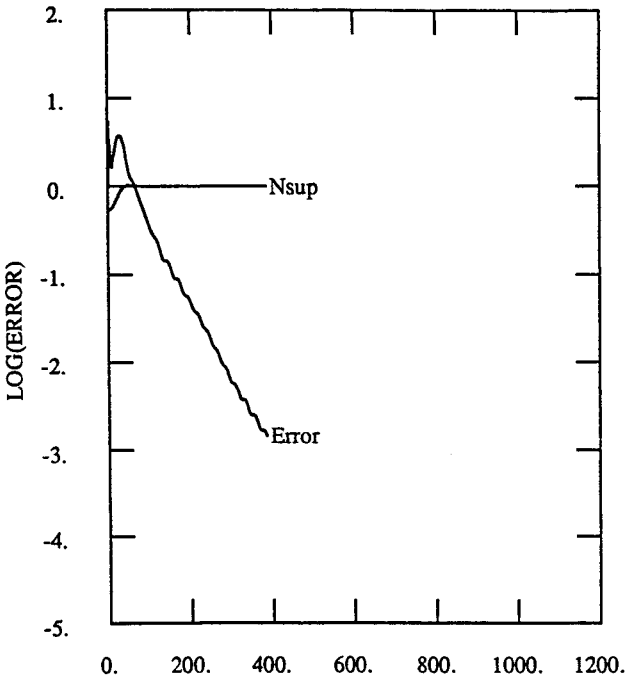

Fig. 15 Convergence history with multigrid.

Fig. 16 Relative Mach number on a blade-to-blade grid plane; rotor 33 compressor, grid 16 × 16 × 64, 85.66% radius.

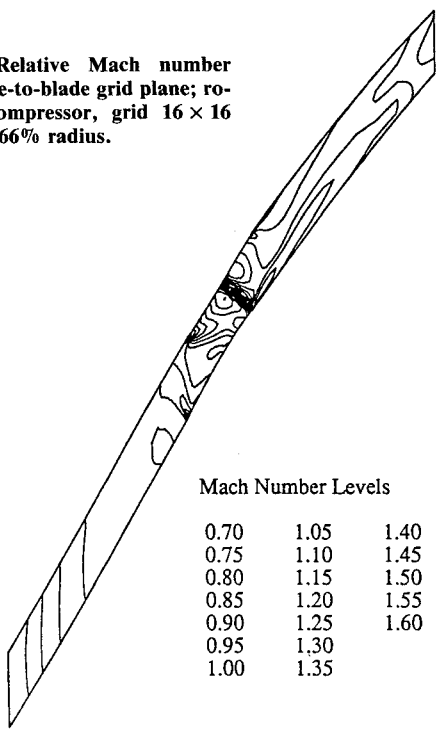

mm, and a hub-to-tip radius ratio of 0.7. Calculations were performed on a $16 \times 16 \times 64$ point H-type mesh (see Fig. 14), again generated using the modified GRAPE code, for a design speed of 16,100 rpm and an exit static-to-inflow total pressure ratio of 1.0. These flow conditions produce a supersonic relative inflow with a subsonic axial flow. The convergence history (see Fig. 15) shows a large correction introduced by the initial conditions, followed by a rapid reduction in the flowfield error. Figures 16 and 17 are qualitative representations of the flowfield in the blade-to-blade and hub-to-shroud planes. A strong passage shock is captured from the midchord of the pressure surface to the trailing edge of the suction surface, whereas a weak shock from the leading ede of the pressure surface impinges onto the rear portion of the suction surface (where the local Mach number is approximately 1.4).

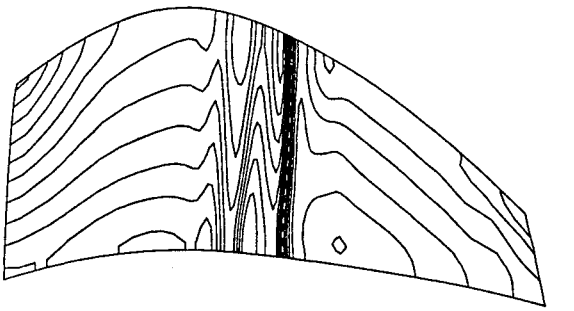

Fig. 17 Relative Mach number on a hub-shroud grid plane; rotor 33 compressor, grid $16 \times 16 \times 64$, 49.88% passage width.

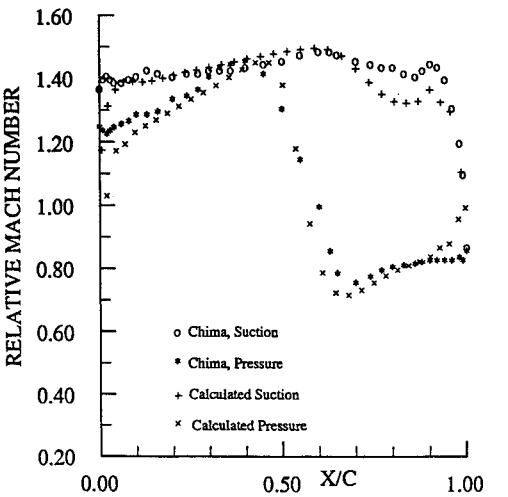

Fig. 18 Relative Mach number blade distribution; rotor 33 compressor, 85.66% radius.

These results compare qualitatively well with the maximum flow calculation produced by Chima and Strazisar[16] using a three-dimensional nonconservative Euler scheme developed by Thompkins.[17] A comparison of the relative Mach number blade distributions at an 85.66% hub-to-shroud radius is seen in Fig. 18. Despite the differences that can be attributed to the conservativeness and nonconservativeness of the two schemes (with possible differences in specified flow conditions), the blade distributions compare quite well.

The unvectorized code was run on a floating point system (FPS) AP-264 processor. Because the point marching nature of the LU scheme, storage requirements can be comparble to those of explicit schemes. This would require the recalculation of the Jacobian matrices at each grid point in both the upper and lower matrix operators at every time step. With this procedure, the CPU time required for one three-level W-cycle multigrid calculation on a $64 \times 16 \times 16$ grid is less than 28 s. The CPU time can be significantly reduced (by 40 to 50%), at the expense of an increased storage requirement, by linearizing the Jacobian matrices over a number of time steps rather than calculating them at every time step.

Conclusions

One can see the benefits the LU scheme has over other implicit methods through a comparison of storage requirements and operation counts. The LU scheme requires only two effectively explicit point-implicit sweeps through the three-dimensional domain as opposed to the three line-implicit sweeps needed in ADI schemes. The LU scheme allows the use of time step sizes larger than those normally permitted in most explicit schemes and, when coupled with the multigrid method, does not suffer from the slower convergence rates often associated with implicit methods. Test cases illustrate the LU implicit scheme's ability to capture three-dimensional flows with reasonable convergence rates. Results show the feasibility of using the LU scheme to solve the three-dimensional Euler equations and its ability to accelerate implicit Euler calculations to steady state when coupled with the multigrid method.

Acknowledgments

This work was supported in part by the NASA Lewis Research Center under Grant NAG 3-645 and by the Natural Sciences and Engineering Research Council of Canada. All computations were run on the Production Supercomputer Facility of the Cornell Center for Theory and Simulation in Science and Engineering, which is funded, in part, by the National Science Foundation, New York State, and the IBM Corporation.

References

[1]Stow, P., "Turbomachinery Blade Design Using Advanced Calculation Methods," *Thermodynamics and Fluid Dynamics of Turbomachinery,* edited by A.S. Ucer, P. Stow, and Ch. Hirsch, NATO ASI Series, Martinus Nijhoff Publishers, Boston, MA, 1985, pp. 923-964.

[2]Jameson, A. and Turkel, E., "Implicit Schemes and LU Decompositions," *Mathematics of Computation,* Vol. 37, Oct. 1981, pp. 385-397.

[3]Buratynski, E.K. and Caughey, D.A., "An Implicit LU Scheme for the Euler Equations Applied to Arbitrary Cascades," *AIAA Journal,* Vol. 24, Jan. 1986, pp. 39-46.

[4]Briley, W.R. and McDonald, H., "Solution of the Three-Dimensional Compressible Navier-Stokes Equation by an Implicit Technique," *Proceedings of the 4th International Conference on Numerical Methods in Fluid Dynamics June 1974, Lecture Notes in Physics,* Vol. 35, Springer-Verlag, New York, 1975, pp. 105-110.

[5]Beam, R.M. an Warming R.F., "An Implicit Finite-Difference Algorithm for Hyperbolic Systems in Conservation Law Form," *Journal of Computational Physics,* Vol. 22, No. 1, Sept. 1976, pp. 87-110.

[6]Pulliam, T.H., "Implicit Finite-Difference Methods for the Euler Equations," *Advances in Computational Transonics,* Vol. 4, edited by W.G. Habashi, Pineridge Press, Swansea, Wales, UK, 1985, pp. 503-575.

[7]Kreiss, H.-O., "Stability Theory for Difference Approximations of Mixed Initial Boundary Value Problems, I," *Mathematics of Computation,* Vol. 22, Oct. 1968, pp. 703-714.

[8]Kreiss, H.-O., "Numerical Methods for Hyperbolic Partial-Differential Equations," *Computational Fluid Dyanmics,* Von Kármán Institute Lecture Series, No. 6, Brussels, Belgium, March 1979.

[9]Rudy, D.H. and Stirkwerda, J.C., "A Nonreflective Outflow Boundary Condition for Subsonic Navier-Stokes Calculations" *Journal of Computational Physics,* Vol. 36, No. 1, June 1980, pp. 55-70.

[10]Jameson, A., "Transonic Flow Calculations for Aircraft, *Lecture Notes in Mathematics,* Vol. 1127, edited by F. Brezzi, Springer-Verlag, New York, 1985, pp. 156-242.

[11]Steger, J.L. and Warming, R.F., "Flux-Vector Splitting of the Inviscid Gasdynamics Equations with Application to Finite-Difference Methods," NASA TM-78605, 1979.

[12]Pan, D. and Lomax, H., "A New Approximate LU Factorization Scheme for the Reynolds-Averaged Navier-Stokes Equations," AIAA Paper 86-0337, Jan. 1986.

[13]South, J.C. and Brandt, A., "Application of a Multi-Level Grid Method to Transonic Flow Calculations," *Transonic Flow Problems in Turbomachinery,* edited by T.C. Adamson and M.F. Platzer, Hemisphere Publishing, Washington, DC, 1977.

[14]Jameson, A. and Yoon, S., "LU Implicit Schemes with Multiple Grids for the Euler Equations," AIAA Paper 86-0105, Jan. 1986.

[15]Sorenson, R., "A Computer Program to Generate Two-Dimensional Grids About Airfoils and Other Shapes by the Use of the Poisson's Equation," NASA TM-81198, 1980.

[16]Chima, R.V. and Strazisar, A.J., "Comparison of Two- and Three-Dimensional Flow Computations with Laser Anemometer Measurements in a Transonic Compressor Rotor," *ASME Journal of Engineering for Power,* Vol. 105, No. 3, July 1983, pp. 596-605.

[17]Thompkins, W.T., Jr., "A FORTRAN Program for Calculating Three-Dimensional Inviscid Rotational Flows with Shock Waves in Axial Compressor Rotors," NASA CR-3560, 1982.